Anisotropic and isotropic light scattering in gaseous low-temperature helium

C. Guillot-Noël, Y. Le Duff, F. Rachet, and M. Chrysos
Laboratoire des Propriétés Optiques des Matériaux et Applications, UMR CNRS 6136,
2, Boulevard Lavoisier, Université d'Angers,
49045 Angers Cedex 01, France
(Received 12 March 2002; published 19 July 2002)

Low-temperature binary collision-induced light-scattering spectra from gaseous helium are reported. Both components, anisotropic and isotropic, are deduced from our measurements and calibrated on an absolute scale. Comparison of the experimental spectra with theoretical profiles computed quantum mechanically is made, by using as input up-to-date interaction potential and incremental polarizability functions. The present study confirms the tendencies we have previously observed at room temperature and strengthens our confidence in certain *ab initio* models.

DOI: 10.1103/PhysRevA.66.012505 PACS number(s): 33.20.Fb, 34.30.+h

I. INTRODUCTION

Research dealing with the light scattered by rare gases in the vicinity of the Rayleigh line has attracted much interest during the last 30 years [1–3]. This is because interaction induced light scattering constitutes a sensitive probe for incremental pair polarizabilities, that is *r*-dependent polarizabilities which are induced by the interaction between two atoms (separated by a distance *r*) in the gaseous sample. Helium is one of the most intriguing candidates, as it forms the lightest of the atomic gases and, thus, the one with the most pronounced quantum behavior. Given its relatively simple structure, it has been the subject of refined quantum mechanical analyses and advanced computational techniques. A variety of analytical [4], semiempirical [5], and *ab initio* [6–9] models have thus far been proposed to describe the two invariants of the interaction-induced polarizability tensor of the helium pair, He_2. Among these models, the ones computed *ab initio* are particularly challenging as they enable one to check, via an effective spectroscopic means, the adequacy of the numerical techniques and to estimate to which extent the quantitative description of the weak interatomic He-He interactions has been satisfactory over the entire *r* domain. One of the most elaborated *ab initio* models is the long-ago-reported Dacre's model [7], obtained through configuration interaction. More recently, two other models were reported, the one by Bishop and Dupuis [9], based on several electron-correlation treatments, and that by Moszynski and co-workers [8], implemented within a symmetry adapted perturbation theory. The comparison between the scattering line shapes, computed from first principles by using these models as an input, and the experimental ones, obtained with a low-density helium sample, can be of decisive importance, especially whenever performed in various thermodynamical conditions.

Several experimental groups have thus far reported binary light-scattering measurements from gaseous helium [10–15]. Yet they have all been limited to a single temperature of the sample, the room temperature. Here, low-temperature (99.6 K) He_2 interaction-induced light-scattering intensities are reported, within the binary collision regime and for frequency shifts attaining 400 cm^{-1}. There are two reasons that motivated the present study: first, that definitive conclusions can be drawn on the validity of the *ab initio* models, once a temperature largely differing from the one checked previously is chosen; second, that at a low temperature the confrontation between theory and experiment must be more challenging, as the quantum nature of helium is expected to show itself more clearly.

The scattering data are collected for two polarizations of the exciting beam, and anisotropic as well as isotropic spectra are deduced on an absolute scale. The comparison of these spectra with theoretical profiles computed quantum mechanically is made according to a fully quantal procedure developed in our institute and by using a modern *ab initio* interatomic potential. The results are examined relative to the recently reported interaction-induced light scattering study of helium at room temperature [13–15].

II. EXPERIMENTAL CONSIDERATIONS

The scattering intensities are measured by using a conventional Raman-scattering setup [15]. In order to excite the sample, the green line ($\lambda = 514.5$ nm) of an argon-ion laser is used, operating at a maximum power of 2 W. A high-pressure four-window cell is employed, built to confine a gaseous sample at pressures of several hundred bars for temperatures ranging from 4 to 300 K. The windows are made of sapphire, which is a uniaxial material. In order to minimize polarization modifications of the light crossing the cell windows, the optical axis of the sapphire crystal is set in a direction perpendicular to the window faces. Before each experimental run, measurements of the depolarization ratio of the $Q_1(J)$ vibrational components of gaseous hydrogen are made and compared with their theoretical values [16], so that any change of the light polarization due to the setup is evaluated. The high-pressure cell is set in a continuous flow cryostat designed by L'Air Liquide for our purposes. The sample temperature is monitored to within accuracies of 1 K by using a calibrated platinum resistance put inside the cell. The light scattered by the gaseous sample is analyzed by means of a double monochromator with two 1800 grooves/mm holographic gratings.

Two sorts of scattering intensities $I_\perp$ and $I_\parallel$ are recorded, corresponding to a polarization of the exciting beam perpendicular ($\perp$) or parallel ($\parallel$) to the scattering plane [17], respec-

tively. A λ/2 plate associated to a glan polarizer is used to switch the polarization of the exciting beam at will. The scattering intensities are calibrated on an absolute scale by using as an external reference either the $S_0(0)$ line of hydrogen or the $S_0(J)$ lines of deuterium [18]. The output data emerging from the monochromator are subjected to several corrections. More specifically, the effects due to the finite aperture of the collected beam are accounted for, as well as the variations of the scattering signal resulting from modifications of the polarization of the light passing through the cell. At each of the probed frequencies, the dependence of the sensitivity of our experimental device—and, in particular, of the photoelectric detector—is also taken into account. In this experiment, two such detectors are employed: a photomultiplier with a bialkali photocathode for the lower-frequency part of the spectra (frequencies not exceeding $\nu = 225\ \mathrm{cm}^{-1}$), and a charged-coupled device for frequencies beyond 225 cm^{-1}, that is, in the far spectral wing where scattering intensities are particularly weak. As has been noted by the authors in a previous paper [15], signals as low as one photoelectron per pixel and per week can so be detected.

III. RESULTS AND DISCUSSION

The scattering intensities are recorded at (99.6 ± 2) K for several densities of the gaseous helium from 40 to 240 amagat. For each of the densities, intensities of the light scattered by the sample are measured for detunings up to $\nu = 400\ \mathrm{cm}^{-1}$. A variable spectral resolution of the monochromator is chosen as a function of ν. For frequencies $\nu \leqslant 20\ \mathrm{cm}^{-1}$ the resolution is fixed to 1.5 cm^{-1}, whereas for larger detunings, widths amounting to 2.5 or 5 cm^{-1} are taken. From these measurements two sorts of total intensities, $I_{\perp,t}$ and $I_{\parallel,t}$, are recorded, corresponding to the $\perp$ and $\parallel$ polarization configurations of the exciting beam, respectively. Then for each ν-value probed and for either polarizations of the exciting beam, the total intensity is expanded in a power series of density, ρ, according to the virial expansion

$$I_t(\nu) = I_0(\nu) + I_1(\nu)\rho + I_2(\nu)\rho^2 + I_3(\nu)\rho^3 + \cdots . \quad (1)$$

Quantities $I_0(\nu)$ and $I_1(\nu)$ designate intensities accounting for parasitic effects (such as noise, fluorescence, Raman bands of impurities) comprised in the expansion through density-independent and linearly dependent terms, respectively. Quantities $I_2(\nu)$ and $I_3(\nu)$ are the two-body and three-body correlation terms, respectively. For each frequency probed, the working density range is chosen so that any term beyond ρ^3 in the series expansion of Eq. (1) is negligible.

Here, we are interested solely in the two-body contribution correlation term $I_2(\nu)$. Following the aforementioned procedure, the two binary components $I_{\perp,2}(\nu)$ and $I_{\parallel,2}(\nu)$ are extracted, according to the choice of the polarization of the incident beam. For the sake of simplicity, in what follows the subscript "2" in the latter two components is dropped and the intensities are denoted as $I_\perp(\nu)$ and $I_\parallel(\nu)$. In Fig. 1, $I_\perp(\nu)$ and $I_\parallel(\nu)$ are plotted on an absolute scale as a function of ν. The former component is reported for frequencies ranging from 5 to 400 cm^{-1}; the latter one corresponds to weaker signals and is given from 5 to 300 cm^{-1}. When compared with the previously reported data for room temperature

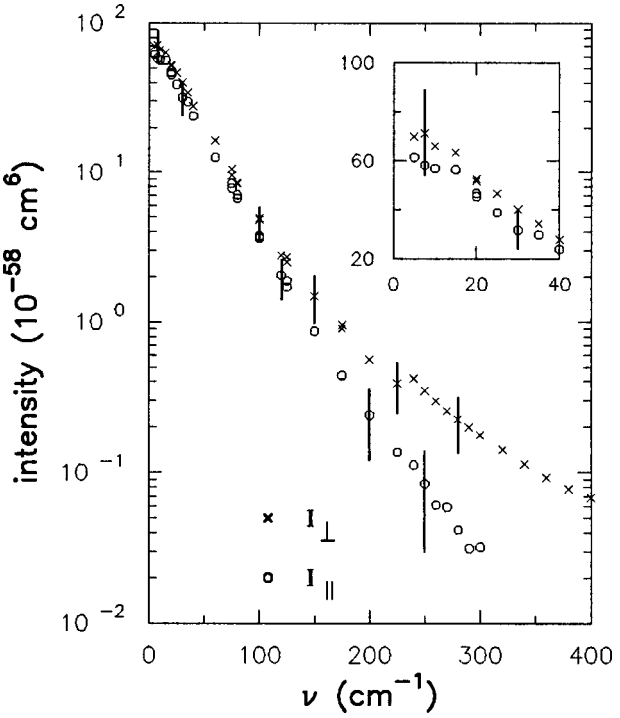

FIG. 1. Low-temperature helium binary $I_\perp$ and $I_\parallel$ intensities, on an absolute scale (cm^6), as a function of frequency ν. Experimental uncertainties are indicated by error bars.

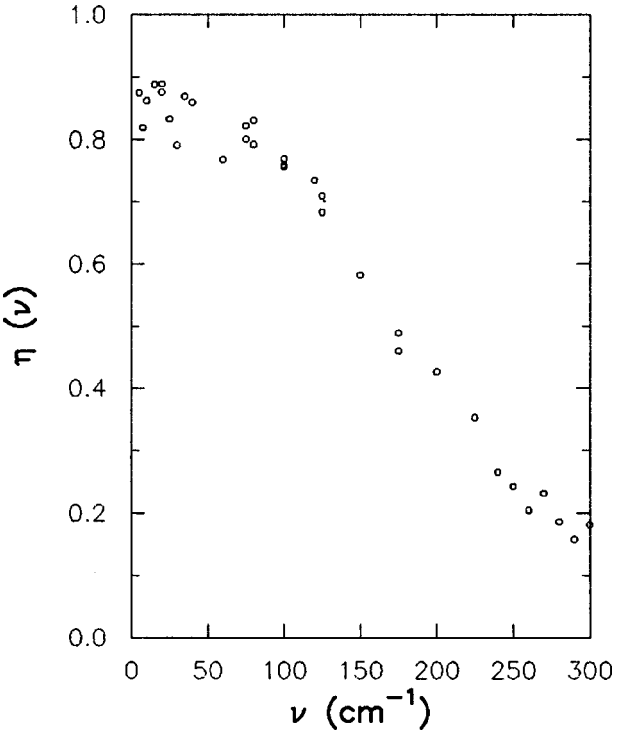

FIG. 2. Helium experimental depolarization ratio η deduced from binary intensities, against ν.

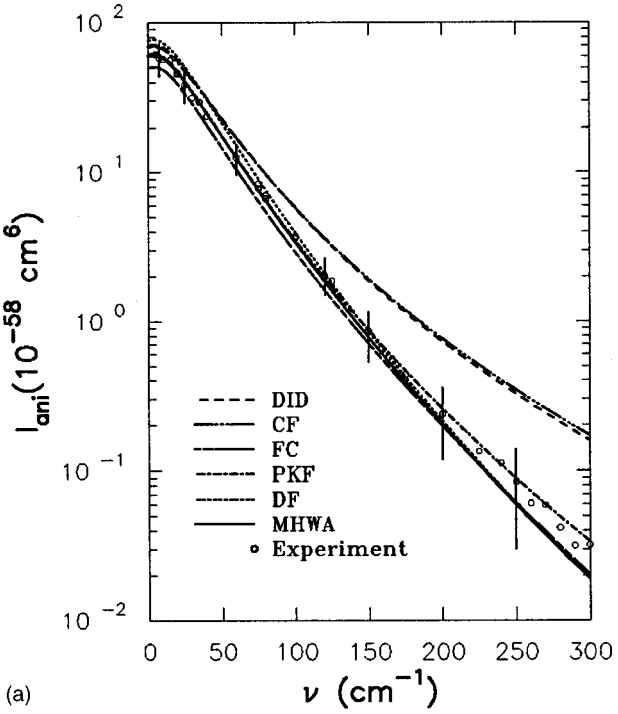

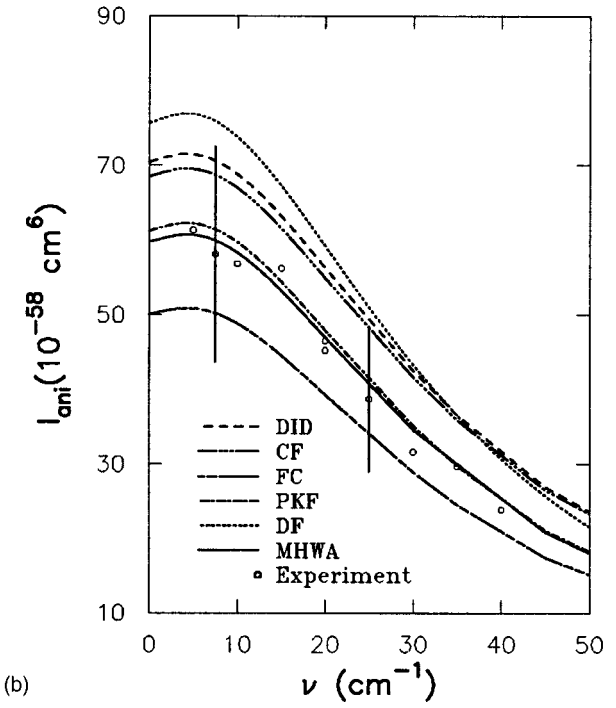

FIG. 3. Comparison between our experimental binary anisotropic spectrum and those obtained quantum mechanically in low-temperature helium. The circles refer to our experiment; uncertainties are indicated by error bars. Curves refer to spectra computed with the following anisotropy models: DID, CF, FC, PKF, DF, and MHWA. Panel (a): spectra plotted on a logarithmic scale over the entire ν domain. Panel (b): enlarged part of the low-frequency domain on a linear scale.

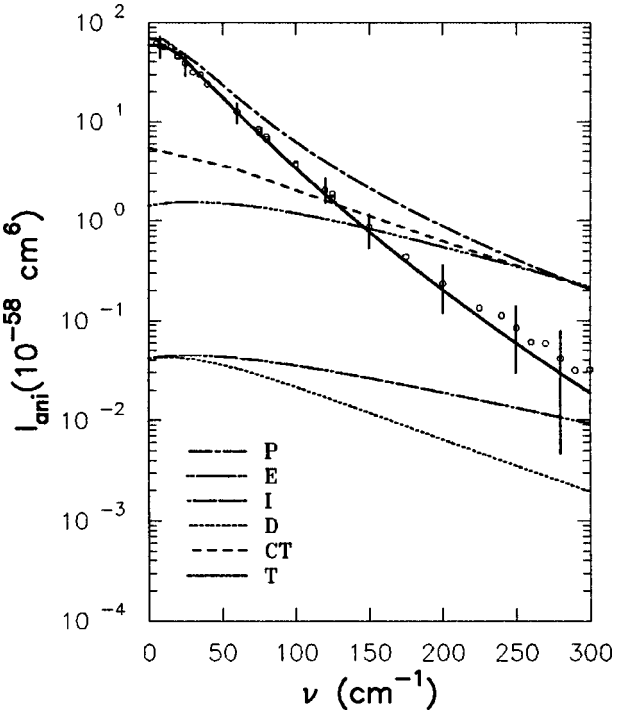

FIG. 4. Partial contributions to the helium anisotropic spectrum computed with the MHWA anisotropy model. The total spectrum (T) is built from the sum of all direct contributions [polarization (P), exchange (E), induction (I), and dispersion (D)] minus twice the cross terms (CT). Our measurements, indicated by circles, are also illustrated for comparison. Experimental uncertainties are indicated by error bars.

[14,15], the helium binary scattering intensities recorded at 99.6 K are found to be higher at low detunings but weaker in the far wing. This feature can been understood as a consequence of the decrease of the atomic velocities in the gas with decreasing temperature. From these scattering intensities the binary depolarization ratio

$$\eta(\nu)=\frac{I_{\parallel}(\nu)}{I_{\perp}(\nu)} \tag{2}$$

can be deduced. In Fig. 2, $\eta(\nu)$ is plotted against ν in the range from 5 to 300 cm^{-1}. At small frequencies ($\nu \leqslant 40\ cm^{-1}$) the value of $\eta(\nu)$ is close to $\frac{6}{7}$, a signature of depolarized scattering [3]. Given that dipole-induced dipole (DID) intensities are well known to be weakly polarized, the classical DID picture is adequate (though only qualitatively) for small frequencies. On the other hand, as ν increases the depolarization ratio progressively decreases, reaching values as low as $\eta \approx 0.2$ at 300 cm^{-1}. This monotonous tendency of the wing to become almost completely polarized with increasing frequencies is the fingerprint of short-range interactions between colliding helium atoms, which strongly contribute to the scattering intensities. It is perhaps noteworthy that at 99.6 K the depolarization ratio does not attain values as low as those observed in our previous work at room tem-

TABLE I. Low-temperature helium binary anisotropic zeroth-order M_0 and second-order M_2 moments calculated with the integral of Eq. (4) (see text). The anti-Stokes spectral intensities were deduced from the Stokes intensities via the *detailed balance principle*. Entries in parentheses denote estimated values deduced from the experimental anisotropic spectrum.

Model	M_0 (10^{-2} Å^9)	M_2 (10^{23} Å^9 sec^{-2})
	Experimental profile	
	(1.46)	(9.35)
	Theoretical profile	
MHWA	1.45	8.82
DF	1.81	10.37
PKF	1.49	9.51
FC	1.22	7.68
CF	1.82	18.47
DID	1.85	18.03

perature [13], where a value $\eta(\nu)\approx 0.03$ was reported, yet in that previous experiment a wider range of frequencies had been probed.

From the two experimental quantities $I_\perp(\nu)$ and $I_\parallel(\nu)$ two spectral components, referred to as the anisotropic $I_{\rm ani}(\nu)$ and isotropic $I_{\rm iso}(\nu)$ intensities, are deduced, through the following expressions that take into account the finite value of the scattered beam aperture angle ($\theta_s \simeq 8°$) [5]:

$$I_{\rm ani}(\nu) = 1.010 I_\parallel(\nu) - 0.010 I_\perp(\nu),$$
$$I_{\rm iso}(\nu) = -1.184 I_\parallel(\nu) + 1.017 I_\perp(\nu). \tag{3}$$

Theoretical profiles are computed by using the up-to-date SAPT1 interaction potential [19] and by employing a highly reliable quantum-mechanical procedure developed in our institute [20]. The wave functions of the continuum are built step by step, according to the Fox-Goodwin propagative method, through outward propagation of the wave-function ratio at every pair of adjacent points defined on a spatial grid ranging from 3 to 150 bohr. A multitude of initial-state energies varied by steps of 15 cm^{-1} and attaining the value of 3000 cm^{-1} are considered. The maximum angular-momentum quantum number is fixed at $J_{\rm max}=300$. These numerical parameters provide convergence of total cross sections to within $<1\%$.

Figure 3 shows our experimental binary anisotropic component $I_{\rm ani}(\nu)$ on an absolute scale (cm^6), as a function of frequency ν ranging between 5 and 300 cm^{-1}. Within this interval, a decrease of the measured intensity by more than three decimal orders is observed. Theoretical profiles are also illustrated in the same figure for various available *ab initio* incremental polarizability models. To start with, the improved anisotropy model of Fortune and Certain (FC) [6], which accounts via *ab initio* computations for the short-distance overlap and exchange effects, systematically underestimates the measured spectrum by about 20%. Yet it responds far better than the—proposed in the 1970's—analytic model of the same authors (CF) [4], which totally fails to reproduce the experiment beyond $\nu\sim 50$ cm^{-1}; this incomplete spectral description and its resemblance with that of the classical DID model—both illustrated for comparison—should be expected, as only long-distance interactions have been taken into account in the earlier Certain and Fortune anisotropy model [4]. The *ab initio* model proposed long ago by Dacre and Frommhold (DF) [7], accounting through self-consistent-field (SCF) and large-scale configuration interaction (CI) computations for short- and long-range effects, is found to be consistent with our measurements above $\nu \simeq 50$ cm^{-1} but below this value it overestimates experiment by about 25%. At this point it should be stressed that there has been a second model, proposed later on by Proffitt, Keto, and Frommhold (PKF) to fit their experimental spectrum at room temperature [5], which—albeit its semiempirical origin—yields a spectral profile in a remarkable agreement with our measurements. Finally, the most up-to-date anisotropy model proposed by Moszynski, Heijmen, Wormer, and van der Avoird (MHWA) [8] and calculated by symmetry adapted perturbation theory was checked, and found to be perfectly consistent with our data both in the wing [Fig. 3(a)] and in the low-frequency part of the spectrum [Fig. 3(b)]. This model has the additional advantage of being able to provide separate anisotropy contributions coming from polarization, exchange, dispersion, and induction mechanisms. The total spectrum is, of course, defined as sum of all the partial intensities, due to the above-mentioned separate terms, and of the cross-term contributions because of their interference. All these contributions are gathered in Fig. 4.

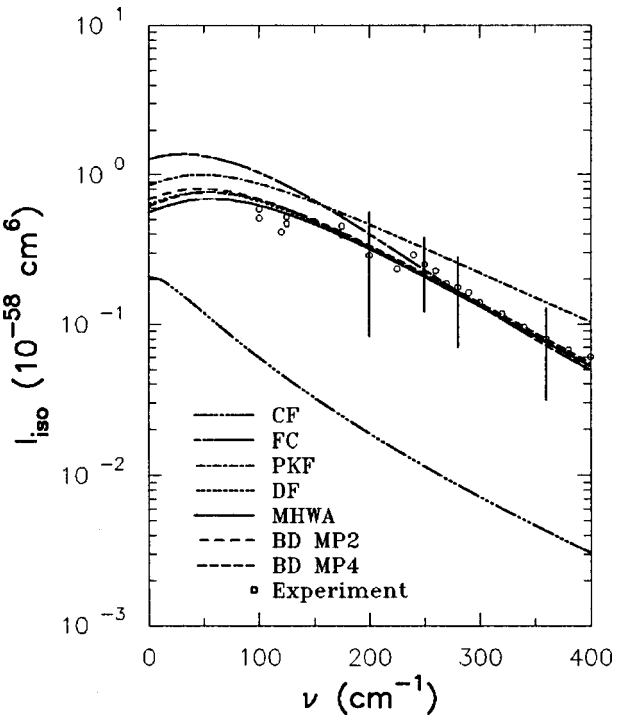

FIG. 5. Comparison between our experimental binary isotropic spectrum and those obtained quantum mechanically in low-temperature helium. The circles refer to our experiment; uncertainties are indicated by error bars. Curves refer to spectra computed with the following incremental trace models: CF, FC, PKF, DF, MHWA, BD-MP2, and BD-MP4.

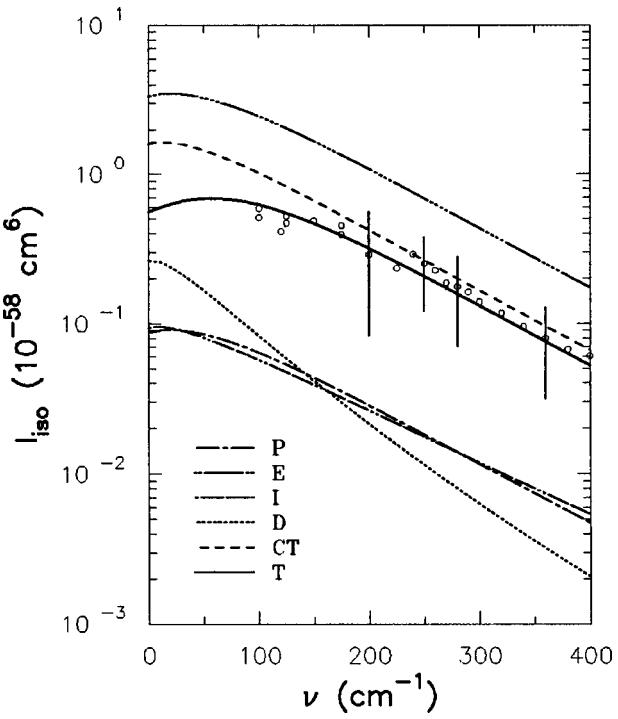

FIG. 6. Partial contributions to the helium isotropic spectrum computed with the MHWA incremental trace model. The total spectrum (T) is built from the sum of all direct contributions [polarization (P), exchange (E), induction (I), and dispersion (D)] minus twice the cross terms (CT). Our measurements, indicated by circles, are also illustrated for comparison. Experimental uncertainties are indicated by error bars.

As is shown in this figure, at low ν, the anisotropic intensities are due mainly to the polarization component, but as ν is increased the exchange term spectral component gets gradually enhanced becoming as intense as the one due to the polarization. The heavy negative mixing of these two components at high values of ν is responsible for the fast attenuation of the anisotropic intensities, in a way analogous to the observations made for room temperature [14].

A global comparison between experimental and theoretical results can be made by determining the zeroth- and second-order moments. With the spectral intensities $I_{\mathrm{ani}}(\nu)$ in cm^6 as input, we are able to deduce these moments, M_0 and M_2, through the following analytical expression:

$$M_{2p}=\frac{15}{2}\left(\frac{\lambda_0}{2\pi}\right)^4\int_{-\infty}^{+\infty}(2\pi c\nu)^{2p}I_{\mathrm{ani}}(\nu)d\nu, \qquad (4)$$

where λ_0 denotes the laser wavelength and p is a nonnegative integer. In our experiment, only the Stokes spectral side is recorded. The anti-Stokes part of the spectrum is deduced by means of the *detailed balance principle*. Table I gives the M_0 and M_2 values estimated from the experimental intensities of the anisotropic spectrum as well as those calculated from the corresponding theoretical spectral profiles. The various entries of the table, and their comparison with the moments extracted from the experimental spectrum, give an indication of the quality of each of the checked models.[1] The conclusions corroborate the ones drawn from the frequency-resolved spectra discussed above.

The much more delicate isotropic spectrum was also measured and computed. Figure 5 illustrates our experimental isotropic spectrum on an absolute scale. No data are reported below 100 cm^{-1} because, in the low-frequency domain, the isotropic spectrum results from the substraction of two almost equal quantities and, thus, is unreliable. Comparison with theoretical profiles obtained quantum mechanically, by use of the same potential as before [19] and incremental traces corresponding to various induced polarizability models, is made. In addition to the incremental trace models determined via the above-mentioned induced polarizability functions [4–8], the *ab initio* Bishop and Dupuis (BD) incremental trace model [9] based on Moller-Plessett perturbation theory on either MP2 and MP4 levels was also checked. The principal conclusion drawn from the comparison is that the four *ab initio* DF [7], MHWA [8], BD-MP2, and BD-MP4 [9] incremental trace spectra are all consistent with each other and perfectly adequate with the experiment throughout the entire domain probed. The profile obtained with the earlier *ab initio* model of FC [6] is less satisfactory, overestimating intensities and revealing a quite different form in the low-frequency part of the spectrum—though remaining inside the (large) experimental error bars. To complete the picture, comparison with the CF [4] and PKF [5] spectral profiles is also made. This comparison shows that the CF profile is totally inconsistent with our measurements, providing us with intensities weaker than the experimental ones by almost one order of magnitude, and that the PKF profile lies systematically above experiment by about 50%.

As now regards partial component analysis, the spectral signature of the polarization, exchange, dispersion, and induction terms, constituting the MHWA incremental trace model, can also be determined in a way analogous to that done above for the anisotropic spectrum. This is displayed in Fig. 6. Beyond $\nu\approx 100$ cm^{-1} the total MHWA isotropic spectrum is found to scale like its two dominant partial contributions, that is the profiles corresponding to the exchange term and its negative couplings with the rest of the trace components.

IV. CONCLUSION

We made an exhaustive experimental and theoretical analysis of binary interaction-induced light scattering in gaseous helium—the less classical of the atomic gases—in thermodynamical conditions expecting to accentuate quantum characteristics possibly revealed by the atomic pair. Our findings reinforced the tendencies observed and the conclu-

[1]At a low temperature, the M_0 and M_2 spectral moments computed with Eq. (4) (see text) were found to largely differ from those extracted through classical radial pair-distribution function integrals. Note that in our previous room-temperature work of Ref. [14] it was these latter integrals which were employed instead, their expressions being given therein by Eqs. (4) and (5) [14].

sions drawn from the previous room-temperature study [13–15], and strengthened our confidence in the latest *ab initio* induced polarizability models for both anisotropy and incremental trace functions. More specifically, the *ab initio* induced polarizability model of Moszynski *et al.*—for which both anisotropy and incremental trace functions are known—was found to be in agreement with experiment whatever the temperature of the sample. This clearly shows that symmetry adapted perturbation theory is an effective tool for calculating optimal interaction induced polarizability models, whose accurate determination plays a crucial role in the quantitative characterization of the weak van der Waals interactions.

[1] M. Thibeau, B. Oksengorn, and B. Vodar, J. Phys. (France) **29**, 287 (1968).

[2] J. P. McTague and G. Birnbaum, Phys. Rev. Lett. **21**, 661 (1968).

[3] L. Frommhold, Adv. Chem. Phys. **46**, 1 (1981).

[4] P. R. Certain and P. J. Fortune, J. Chem. Phys. **55**, 5818 (1971).

[5] M. H. Proffitt, J. W. Keto, and L. Frommhold, Can. J. Phys. **59**, 1459 (1981).

[6] P. J. Fortune and P. R. Certain, J. Chem. Phys. **61**, 2620 (1974).

[7] P. D. Dacre and L. Frommhold, J. Chem. Phys. **76**, 3447 (1982).

[8] R. Moszynski, T. G. A. Heijmen, P. E. S. Wormer, and Ad van der Avoird, J. Chem. Phys. **104**, 6997 (1996).

[9] D. P. Bishop and M. Dupuis, Mol. Phys. **88**, 887 (1996).

[10] F. Barocchi, P. Mazzinghi, and M. Zoppi, Phys. Rev. Lett. **41**, 1785 (1978).

[11] M. H. Proffitt and L. Frommhold, Phys. Rev. Lett. **42**, 1473 (1979); L. Frommhold and M. H. Proffitt, J. Chem. Phys. **70**, 4803 (1979).

[12] Y. Le Duff, Phys. Rev. A **20**, 48 (1979).

[13] F. Rachet, M. Chrysos, C. Guillot-Noël, and Y. Le Duff, Phys. Rev. Lett. **84**, 2120 (2000).

[14] C. Guillot-Noël, M. Chrysos, Y. Le Duff, and F. Rachet, J. Phys. B **33**, 569 (2000).

[15] F. Rachet, Y. Le Duff, C. Guillot-Noël, and M. Chrysos, Phys. Rev. A **61**, 062501 (2000).

[16] W. Holzer, Y. Le Duff, and K. Altmann, J. Chem. Phys. **58**, 642 (1973).

[17] The scattering plane is defined by the laser beam and the average axis of the collected by the monochromator scattering beam.

[18] F. Chapeau-Blondeau, V. Teboul, J. Berrué, and Y. Le Duff, Phys. Lett. A **173**, 153 (1993).

[19] A. R. Janzen and R. A. Aziz, J. Chem. Phys. **107**, 914 (1997).

[20] M. Chrysos, O. Gaye, and Y. Le Duff, J. Phys. B **29**, 583 (1996).